Absence of Melatonin Induces Night-Time Hepatic Insulin Resistance and Increased Gluconeogenesis Due to Stimulation of Nocturnal Unfolded Protein Response

Tatiane C. Nogueira,* Camilo Lellis-Santos,* Daniel S. Jesus, Marco Taneda, Sandra C. Rodrigues, Fernanda G. Amaral, Ana Maria S. Lopes, José Cipolla-Neto, Silvana Bordin, and Gabriel F. Anhê

Department of Physiology and Biophysics (T.C.N., C.L.-S., D.S.J., M.T., S.C.R., F.G.A., A.M.S.L., J.C.-N., S.B.), Institute of Biomedical Sciences, University of Sao Paulo, Sao Paulo 05508-900, Brazil; and Department of Pharmacology (G.F.A.), Faculty of Medical Sciences, State University of Campinas, Campinas 13084-971, Brazil

It is known that the circadian rhythm in hepatic phosphoenolpyruvate carboxykinase expression (a limiting catalytic step of gluconeogenesis) and hepatic glucose production is maintained by both daily oscillation in autonomic inputs to the liver and night feeding behavior. However, increased glycemia and reduced melatonin (Mel) levels have been recently shown to coexist in diabetic patients at the end of the night period. In parallel, pinealectomy (PINX) is known to cause glucose intolerance with increased basal glycemia exclusively at the end of the night. The mechanisms that underlie this metabolic feature are not completely understood. Here, we demonstrate that PINX rats show night-time hepatic insulin resistance characterized by reduced insulin-stimulated RAC-α serine/threonine-protein kinase phosphorylation and increased phosphoenolpyruvate carboxykinase expression. In addition, PINX rats display increased conversion of pyruvate into glucose at the end of the night. The regulatory mechanism suggests the participation of unfolded protein response (UPR), because PINX induces night-time increase in activating transcription factor 6 expression and prompts a circadian fashion of immunoglobulin heavy chain-binding protein, activating transcription factor 4, and CCAAT/enhancer-binding protein-homologous protein expression with Zenith values at the dark period. PINX also caused a night-time increase in Tribble 3 and regulatory-associated protein of mammalian target of rapamycin; both were reduced in liver of PINX rats treated with Mel. Treatment of PINX rats with 4-phenyl butyric acid, an inhibitor of UPR, restored night-time hepatic insulin sensitivity and abrogated gluconeogenesis in PINX rats. Altogether, the present data show that a circadian oscillation of UPR occurs in the liver due to the absence of Mel. The nocturnal UPR activation is related with night-time hepatic insulin resistance and increased gluconeogenesis in PINX rats. **(*Endocrinology* 152: 1253–1263, 2011)**

Melatonin (Mel) production by pineal gland modulates carbohydrate metabolism in such way that pinealectomy (PINX) leads to glucose intolerance and insulin resistance (1). The impairment of insulin-induced glucose uptake by adipocytes is one feature that accounts for whole-body insulin resistance in PINX rats. Importantly, insulin resistance is detected in both phases of the light-dark cycle (L/D cycle) (2). PINX also promotes a dark period-specific increase in basal glycemia that is reversed by Mel reposition, irrespective of an *ad libitum* or scheduled feeding regimen (3). Increased night-time glu-

ISSN Print 0013-7227 ISSN Online 1945-7170
Printed in U.S.A.

doi: 10.1210/en.2010-1088 Received September 20, 2010. Accepted January 18, 2011.
First Published Online February 8, 2011

* T.C.N. and C.L.-S. contributed equally to this work.

Abbreviations: AKT, RAC-α serine/threonine-protein kinase; ATF, activating transcription factor; AUC, area under the curve; CHOP, CCAAT/enhancer-binding protein-homologous protein; ER, endoplasmatic reticulum; FoxO1, forkhead box protein O1; ipPTT, ip pyruvate tolerance test; IRE1, inositol-requiring protein 1; L/D cycle, light-dark cycle; Mel, melatonin; 3-mpa, 3-mercaptopicolinic acid; mTOR, target of rapamycin; PBA, 4-phenyl butyric acid; PEPCK, phosphoenolpyruvate carboxykinase; PINX, pinealectomy; PINX+Mel, PINX receiving nocturnal Mel reposition in the drinking water; PINX+PBA, PINX receiving PBA; RAPTOR, regulatory-associated protein of mTOR; SHAM, sham operated; TRB3, Tribble 3; UPR, unfolded protein response; ZT, Zeitgeber time.

cose concentration in PINX rats occurs even in the presence of higher levels of insulin secretion at the night (4), which suggests that an additional territory contributes to the night time-related insulin resistance when Mel is absent.

Ii is well known that the liver is a key organ that releases glucose into the circulation by means of glycogenolysis and gluconeogenesis, to maintain glycemia into a close range. The limiting step of hepatic gluconeogenesis is the enzymatic activity of phosphoenolpyruvate carboxykinase (PEPCK), which expression is controlled by insulin (5). In rats, a circadian rhythm in hepatic PEPCK expression and hepatic glucose production is maintained by both daily oscillation in autonomic inputs to the liver and night feeding behavior (6, 7). Pointing to a putative endocrine control of circadian regulation of hepatic glucose production, it has been demonstrated that diabetic patients show increased gluconeogenesis and hyperglycemia during the first morning hours, in parallel to decreased levels of circulating Mel (8). Whether an alteration in circadian rhythm of hepatic gluconeogenesis or PEPCK expression contributes to the increased night-time hyperglycemia induced by the absence of Mel remains to be determined.

During the last few years, it has become clear that the endoplasmatic reticulum (ER) participates in the genesis of diabetes by activating an unfolded protein response (UPR) as a consequence of unfolded or misfolded protein accumulation within the ER lumen (9). UPR activation has been reported to induce both pancreatic β-cell death and insulin resistance (10–12). Importantly, short-term UPR activation in the liver was shown to result in an increase in glucose production (13, 14).

In the present study, we investigated the expression profile of key intracellular mediators of the UPR throughout the L/D cycle in the liver of sham-operated (SHAM) and PINX rats supplemented or not with Mel. These parameters were assessed together with the expression and activity of signaling proteins and metabolic enzymes classically correlated with the regulation of hepatic gluconeogenesis by insulin. Hepatic insulin resistance was assessed by measuring the ability of insulin in acutely stimulate RAC-α serine/threonine-protein kinase (AKT) phosphorylation, and gluconeogenesis was estimated by ip pyruvate tolerance test (ipPTT).

Materials and Methods

Animals, surgical procedure, Mel supplementation, and treatment with 4-phenyl butyric acid (PBA)

Wistar rats obtained from the Animal Breeding Center of the Institute of Biomedical Sciences (Sao Paulo, Brazil) were kept under strictly light cycle conditions (12-h light, 12-h dark cycle) with free access to food and water. Seven-week-old rats were anesthetized with ip injection of sodium thiopental (50 mg/kg body weight) and subjected to PINX or to a SHAM, according to the method previously described (15). Briefly, the anesthetized animal was placed in a stereotaxic apparatus for small animals, and a sagittal opening was made on the scalp. The skin and muscles were pushed aside to expose the λ suture. By means of a circular drill, a disc-shaped perforation was made around the λ, and the disc-shaped piece of bone was delicately removed. Thereafter, the pineal gland (which is located just below the posterior venous sinus confluence) was removed with a fine forceps. Afterward, the skull was closed by returning the disc-shaped bone, and the scalp was sutured with cotton thread.

After recovery from surgery, rats were provided with food and water *ad libitum* (one animal per cage). A separated group of animals submitted to PINX received nocturnal Mel (Sigma Chemical Co., St. Louis, MO) reposition in the drinking water (PINX+Mel) as previously described (16). Six weeks after surgery, rats were euthanized at different Zeitgeber times (ZTs) (3, 6, and 9 h after lights on: ZT3, ZT6, and ZT9, respectively, and 0, 3, 6, 9, and 12 h after lights off: ZT12, ZT15, ZT18, ZT21, and ZT24, respectively). After all experiments, effectiveness of the PINX was verified by the macroscopic *post mortem* examination of the central nervous system to check for pineal absence.

PBA (Sigma-Aldrich, St. Louis, MO) was diluted in vehicle [0.9% NaCl (wt/vol) and 0.15 mM $NaHCO_3$] to a final concentration of 100 mg/ml. PINX rats received PBA (PINX+PBA) or vehicle ip during 7 d prior the experimental procedure. In these experiments, SHAM rats were treated with vehicle. PBA dosage was 250 $mg/Kg^{-1}{\cdot}d^{-1}$ injected at ZT12. All experiments were conducted in accordance with the guidelines of the Brazilian College for Animal Experimentation and were approved by the Institute of Biomedical Sciences Ethics Committee for Animal Research.

Intraperitoneal PTT

Rats were fasted for 12 h, and a sodium pyruvate solution (250 mg/ml) was injected ip at ZT24. The final dosage of pyruvate was 2 g/kg. Glucose was determined in blood extracted from the tail before (0 min) and 15, 30, 60, 90, 120, and 150 min after pyruvate injection. The area under the curve (AUC) glycemia *vs.* time was calculated above each individual baseline (basal glycemia) to estimate the total glucose synthesized from pyruvate. Control experiments were performed in PINX and SHAM rats with an oral administration of 3-mercaptopicolinic acid (3-mpa) (30 mg/kg), an inhibitor of gluconeogenesis, 30 min before pyruvate injection.

RNA extraction and RT-PCR

Total RNA was extracted from approximately 100 mg of liver of SHAM and PINX rats using Trizol reagent (Invitrogen, Carlsbad, CA). Total RNA was reverse transcribed for both end-point and real-time PCR. End-point PCR was performed as previously described (17). The amplification products were run on a 1.0% agarose gel containing ethidium bromide, and band intensities were determined by digital scanning followed by quantification using the Scion Image analysis software (Scion Corp., Frederick, MD). The results were expressed as a ratio of the target genes by the housekeeping ribosomal protein L37a. The primer sequences used for end-point RT-PCR analysis with their respective annealing temperature are described in Supplemental Table 1, published on The Endocrine Society's Journals Online web site at http://endo.endojournals.org.

Real-time PCR was performed to detect Tribble 3 (*trb3*), regulatory-associated protein of mammalian target of rapamycin (mTOR) (*raptor*), *pepck*, and forkhead box protein O1 (*foxo1*) mRNA expression using Stratagene Mx4000 equipment (Agilent Technologies, Santa Clara, CA) and Sybr Green as fluorescent dye (Invitrogen). Primer sequences and annealing temperature are described in Supplemental Table 2. Amplification efficiency of each sample was calculated as previous described (18), and relative gene expression was determined by the method described by Liu and Saint (19) using ribosomal protein L37a as inner control. All samples were compared using the relative cycle threshold.

Protein extraction and immunoblotting

For insulin signaling experiments, rats were anesthetized with sodium thiopental (5 mg/100 g body weight ip). The abdominal cavity was opened, and a fragment of the liver was removed to assess basal AKT phosphorylation. Next, the cava vein was exposed and injected with 0.1 ml of a 10^{-4} M insulin solution. After 30 sec, an additional fragment of the liver was removed to assess insulin-stimulated AKT phosphorylation. For protein expression and phosphorylation along the L/D cycle, rats were anesthetized, and a fragment of the liver was removed. Liver samples were processed for Western blotting as previously described (17). Primary antibodies used were: CCAAT/enhancer-binding protein-homologous protein (CHOP), activating transcription factor (ATF)4, phospho-AKT1/2/3 (Ser473), TRB3, PEPCK (Santa Cruz Biotechnology, Inc., Santa Cruz, CA), AKT1, AKT2 (Upstate Biotechnology, New York, NY), rapamycin-insensitive companion of mTOR and RAPTOR (Cell Signaling Technology, Lake Placid, NY), and phospho-eiF2α (Ser51) (Abcam, Cambridge, MA). A secondary antibody conjugated with horseradish peroxidase (Bio-Rad, Hercules, CA) was used followed by chemiluminescent detection of the bands in x-ray sensitive films. Optical densitometry of the films was performed using the Scion Image analysis software (Scion Corp.).

Statistical analysis

Data are presented as mean ± SE. Temporal variation along the 24 h, for each group (SHAM and PINX), was evaluated using one-way ANOVA with Tukey *post hoc* test, after checking for normality of the data. Comparisons between the 24-h profiles were performed using two-way ANOVA, considering as factors "time of the day" (ZT) and "surgery" (SHAM and PINX groups) followed by the Bonferroni *post hoc* test. Two-way ANOVA followed by the Bonferroni was also used to compare SHAM, PINX, and PINX treated with Mel within the same ZT.

The 24-h means for some variables of CTL and PINX groups were compared either using standard *t* test or Mann-Whitney, according to the results of D'Agostino-Pearson normality test. All graphs and statistical tests were done using GraphPad Prism version 5.03 for Windows (GraphPad Software, San Diego, CA).

Results

Body weight, adiposity, and food intake

Body weight and adiposity were equal between SHAM and PINX rats. Mean body weight was 368.80 ± 13.07 g for SHAM and 366.30 ± 19.30 g for PINX rats. Mean adiposity (estimated by the ratio between periepididymal fat depot and body weight) was 13.40 ± 0.30 mg/g for SHAM and 13.60 ± 1.40 mg/g for PINX rats (Supplemental Table 3). Food intake was assessed during the light and dark phases of L/D cycle. Values were equal for PINX and SHAM in both diurnal and nocturnal periods (Supplemental Fig. 1).

Nocturnal profile of AKT expression and phosphorylation in liver of SHAM and PINX rats

AKT content and phosphorylation were assessed in liver of SHAM and PINX rats at several points of the dark phase and at a representative diurnal point (ZT6) of the L/D cycle. Representative blots are shown in Fig. 1A.

AKT phosphorylation was reduced in PINX compared with SHAM rats at ZT18 and at ZT21 (0.63- and 0.67-fold of SHAM, respectively; $P < 0.05$). The opposite pattern was observed at ZT6, *i.e.* AKT phosphorylation in PINX was 2.2-fold of that found in SHAM rats ($P < 0.05$). In addition, PINX rats exhibited the highest levels of AKT phosphorylation at ZT6 (2.03-fold of ZT18; $P < 0.05$), whereas SHAM exhibited it at ZT21 (1.80-fold of ZT24; $P < 0.05$) (Fig. 1B). Nocturnal Mel reposition restored AKT phosphorylation in PINX liver at ZT18, reaching values similar of that found in SHAM animals. Addition of vehicle in drinking water did not interfere with the reduction of hepatic AKT phosphorylation in PINX rats (0.73-fold of SHAM; $P < 0.05$) (Fig. 1E).

AKT1 protein content was kept constant in both SHAM and PINX rats during the same sampling points (Fig. 1C). On the other hand, AKT2 expression showed a circadian pattern. In SHAM animals it peaked at ZT6 (2.2-fold of SHAM at ZT24; $P < 0.05$). In PINX rats, maximal values were detected at ZT18 (1.7-fold of SHAM; $P < 0.05$) and lower levels at ZT15 (Fig. 1D).

PINX rats display hepatic insulin resistance and increased gluconeogenesis at ZT24

A putative physiological significance for reduced AKT phosphorylation was investigated by analyzing gluconeogenesis through ipPTT. Compared with SHAM, pyruvate load induced a higher increase in blood glucose in PINX rats (Fig. 2A). This response was significantly higher at 30, 60, 90, and 120 min after pyruvate injection and resulted in 3.10-fold increase ($P < 0.05$) in the AUC (Fig. 2B). PINX rats treated with Mel exhibited glucose levels similar to SHAM rats.

To verify if the increase in circulating glucose levels after ipPTT were actually due to gluconeogenesis, SHAM and PINX rats were previously treated with 3-mpa, an inhibitor of PEPCK. Pretreatment with 3-mpa completely inhibited the increase in glycemia in-

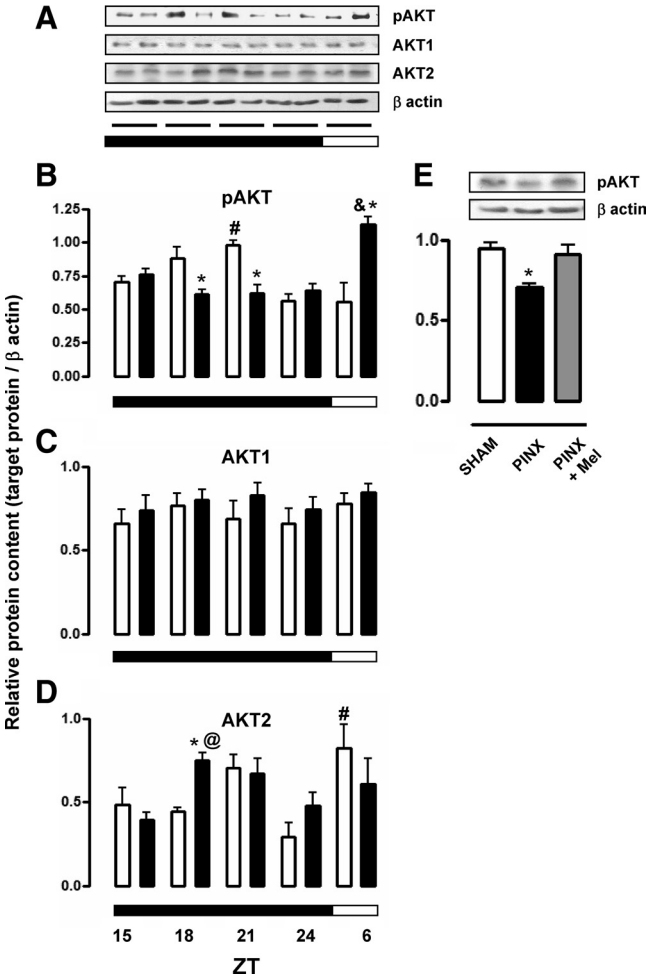

FIG. 1. Nocturnal profile of AKT phosphorylation and expression in liver of SHAM and PINX rats. SHAM (*white bars*) and PINX (*black bars*) rats were housed in 12-h light, 12-h dark cycle under *ad libitum* feeding conditions and killed at the indicated ZT times (ZT6, ZT15, ZT18, ZT21, and ZT24). A fragment of the liver was removed and processed for immunoblotting detection of phosphoAKT, AKT1, AKT2, and β-actin (A). Data of pAKT (B), AKT1 (C), and AKT2 (D) were normalized by those of β-actin. PINX+Mel rats (*gray bars*) were killed at ZT18, and a fragment of the liver was removed and processed for immunoblotting detection of pAKT and β-actin. In this case, SHAM and PINX rats killed at ZT18 were treated with vehicle. Data of pAKT were normalized by those of β-actin (E). Results are shown as mean ± SE.*, $P < 0.05$ *vs.* SHAM at the same ZT; #, $P < 0.05$ *vs.* SHAM at ZT24; &, $P < 0.05$ *vs.* PINX at ZT18; @, $P < 0.05$ *vs.* PINX at ZT15 (n = 6).

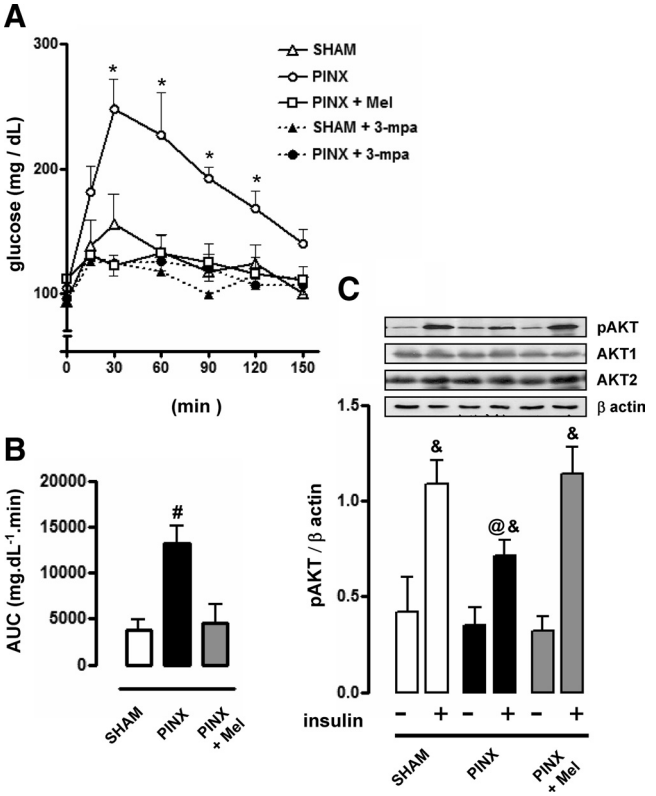

FIG. 2. Gluconeogenesis and insulin-stimulated AKT phosphorylation in liver of SHAM, PINX, and PINX+Mel rats. Intraperitoneal PTT was performed in SHAM, PINX, and PINX+Mel rats at ZT24. Blood was collected from the tail before (0 min) and 15, 30, 60, 90, 120, and 150 min after pyruvate injection. SHAM and PINX rats were also pretreated with 3-mpa (A). The AUC was calculated for each individual animal within the groups SHAM, PINX, and PINX+Mel (B). SHAM, PINX, and PINX+Mel rats were anesthetized, and a fragment of the liver was removed at ZT24. Insulin injection was given in the cava vein, and another liver fragment was removed 30 sec later. Samples were used for immunoblotting detection of pAKT, AKT1, AKT2, and β-actin. Data of pAKT were normalized by those of β-actin (C). Results are shown as mean ± SE. *, $P < 0.05$ *vs.* SHAM at the same time point after pyruvate load; #, $P < 0.05$ *vs.* SHAM; &, $P < 0.05$ *vs.* basal pAKT within the same group; @, $P < 0.05$ *vs.* insulin stimulated pAKT of SHAM (n = 6).

duced by pyruvate in both PINX and SHAM animals (Fig. 2A), assuring the gluconeogenic component of the ascending curve.

Basal AKT phosphorylation was similar in SHAM and PINX rats at ZT24. Insulin efficiently stimulated AKT phosphorylation in all groups (2.59-fold for SHAM, 2.00-fold for PINX, and 3.2-fold for PINX+Mel; $P < 0.05$). However, insulin-stimulated AKT phosphorylation in PINX was lower (0.73-fold *vs.* SHAM; $P < 0.05$) but was recovered after Mel reposition (Fig. 2C).

Absence of Mel alters night-time expression of liver FoxO1 and PEPCK

Foxo1 and *pepck* mRNA expression were assessed in liver of SHAM and PINX rats during the dark phase of the L/D cycle, as well as at a representative diurnal ZT (ZT6). The expression of *foxo1* mRNA in liver of SHAM rats was maximal at ZT21, representing more than 3-fold of the lowest value seen at ZT24 ($P < 0.05$). On the other hand, *foxo1* expression in liver of PINX rats peaked at ZT18 (3-fold increase *vs.* ZT24; $P < 0.05$). Comparing these two nocturnal profiles, PINX showed values of *foxo1* mRNA expression 1.9-fold higher than SHAM at ZT18 ($P < 0.05$). At the diurnal ZT6, however, *foxo1* expression was 1.2-fold higher in SHAM than in PINX ($P < 0.05$) (Fig. 3A). FoxO1 protein content in PINX at ZT18 was also higher in SHAM (1.4-fold; $P < 0.05$). Similar to our pre-

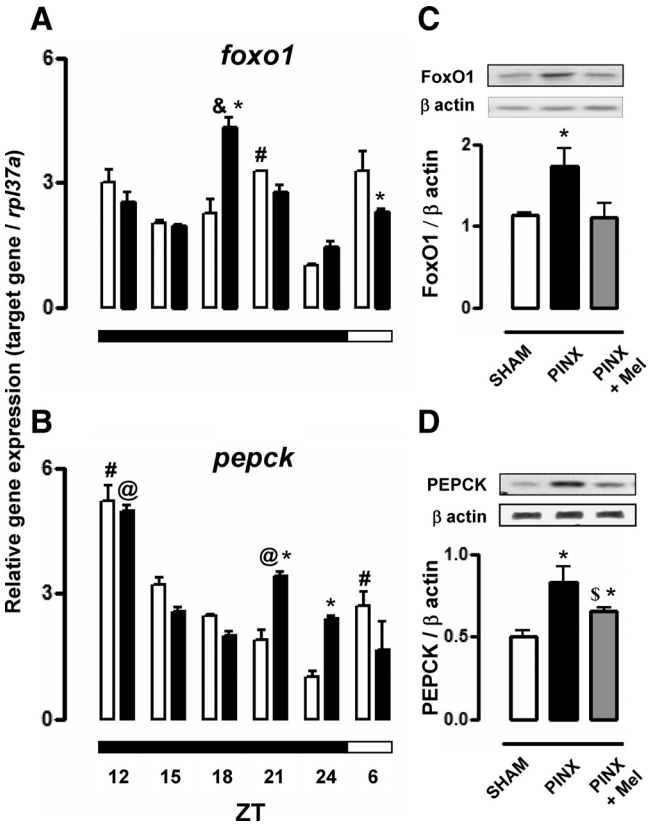

FIG. 3. Nocturnal profile of *pepck* and *foxo1* expression in liver of SHAM and PINX rats. SHAM (*white bars*) and PINX (*black bars*) rats were housed in 12-h light, 12-h dark cycle under *ad libitum* feeding conditions and killed at the indicated ZT times (ZT6, ZT12, ZT15, ZT18, ZT21, and ZT24). A fragment of the liver was removed and processed for total RNA extraction and *foxo1* (A) and *pepck* (B) mRNAs detection by real-time PCR. SHAM, PINX, and PINX+Mel (*gray bars*) were also killed at ZT18 and ZT24, and a fragment of the liver was removed and processed for immunoblotting detection of FoxO1 (C) and PEPCK (D), respectively. In both cases, membranes were probed with β-actin, which was used for data normalization. Results are shown as mean ± SE.*, $P < 0.05$ *vs.* SHAM at the same ZT; #, $P < 0.05$ *vs.* SHAM at ZT24; &, $P < 0.05$ *vs.* PINX at ZT24; @, $P < 0.05$ *vs.* PINX at ZT18; $, $P < 0.05$ *vs.* PINX at ZT24 (n = 6).

vious results, Mel treatment resumed FoxO1 content to SHAM levels (Fig. 3C).

SHAM nocturnal profile of *pepck* mRNA showed a monomodal curve peaking at ZT12 (2.9-fold of ZT24 values; $P < 0.05$). In these animals, we also observed a diurnal increase at ZT6 when compared with ZT24 (2.71-fold; $P < 0.05$). On the other hand, PINX induced a bimodal curve of *pepck* mRNA peaking at ZT12 and ZT21. Also, *pepck* expression was higher in PINX when compared with SHAM at ZT21 and ZT24 (1.80- and 2.40-fold, respectively; $P < 0.05$) (Fig. 3B). Accordingly, we found that PEPCK protein content was increased 1.74-fold in liver of PINX rats when compared with SHAM at ZT24 ($P < 0.05$). Mel treatment did not restore PEPCK levels at ZT24 but reduced it when compared with PINX animals that received the vehicle (0.79-fold the values of vehicle-treated PINX animals; $P < 0.05$) (Fig. 3D).

Effect of PINX on daily *atf6*, *chop*, *atf4*, *bip*, *perk*, and *xbp-1* mRNA profiles

The daily profile of *atf6* expression in SHAM rats did not show a significant variation along the L/D cycle. In spite of this, the nocturnal expression was smaller than the diurnal expression (Mann-Whitney *U* test; $P < 0.05$). This pattern of daily fluctuation was modified by PINX. PINX rats showed significant variation along the L/D cycle ($P < 0.05$), and a bimodal pattern of *atf6* mRNA was detected peaking at ZT15 and ZT21. The comparison with SHAM revealed that PINX animals have increased *atf6* expression at ZT15 (1.70-fold of SHAM values; $P < 0.05$) and at ZT21 (1.80-fold of SHAM values; $P < 0.05$) (Fig. 4A).

The expression of *chop* in SHAM rats did not show a significant variation along the L/D cycle. However, PINX induced the appearance of a significant variation along the

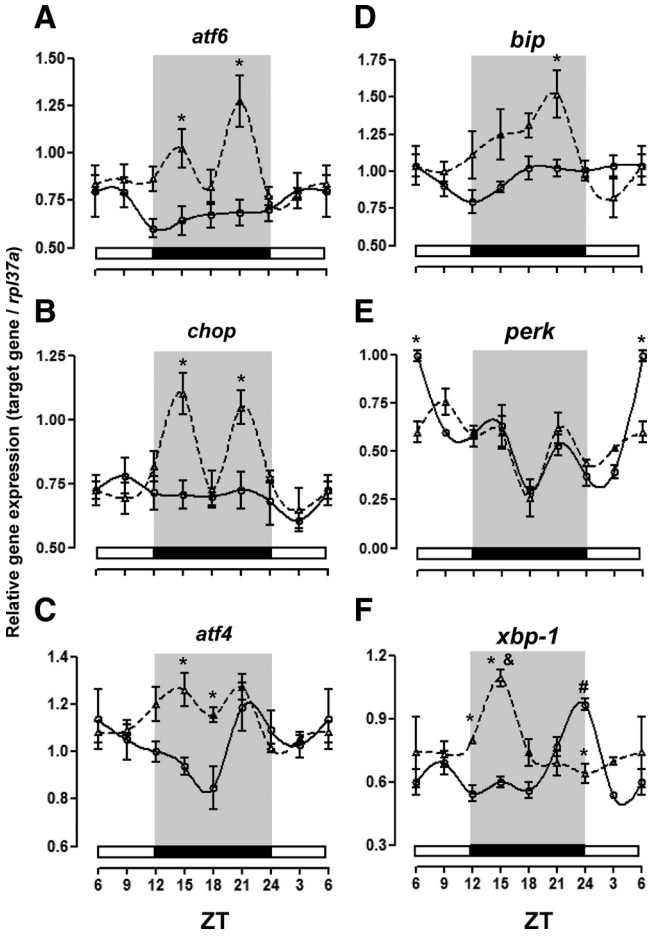

FIG. 4. L/D cycle profile of *atf6*, *chop*, *atf4*, *bip*, *perk*, and *xbp-1* mRNA levels in liver of SHAM and PINX rats. SHAM (*lines with circles*) and PINX (*lines with triangles*) rats were housed in 12-h light, 12-h dark cycle under *ad libitum* feeding conditions and killed at the indicated ZT times (ZT3, ZT6, ZT9, ZT12, ZT15, ZT18, ZT21, and ZT24). *White and black bars* indicate, respectively, the light and dark phases of the L/D cycle. A fragment of the liver was removed and processed for total RNA extraction and *atf6* (A), *chop* (B), *atf4* (C), *bip* (D), *perk* (E), and *xbp-1* (F) mRNAs detection by end-point PCR. Results are shown as mean ± SE. *, $P < 0.05$ *vs.* SHAM at the same ZT; #, $P < 0.05$ *vs.* SHAM at ZT9; &, $P < 0.05$ *vs.* PINX at ZT9 (n = 4).

L/D cycle ($P < 0.05$). Daily *chop* expression in PINX rats showed a bimodal pattern peaking at ZT15 and ZT21. Our data show that *chop* mRNA was higher in PINX at ZT15 and ZT21 when compared with SHAM (1.60- and 1.50-fold of SHAM values, respectively; $P < 0.05$) (Fig. 4B).

In SHAM rats, *atf4* expression reached lowest values in the middle of the night (ZT18) and at ZT21. Pineal ablation changed the daily profile of *atf4* mRNA expression to a bimodal curve peaking at ZT15 and ZT21. Our data revealed that *atf4* mRNA expression in PINX rats was significantly higher at ZT15 and ZT18 when compared with SHAM (1.40- and 1.30-fold of SHAM values, respectively; $P < 0.05$) (Fig. 4C).

The mean hepatic *bip* mRNA expression along the 24 h of the L/D cycle was higher in PINX when compared with SHAM rats ($P < 0.05$). This difference was best seen during the night and was maximal at ZT21 (1.50-fold of SHAM; $P < 0.05$). The daily profile of *bip* expression in SHAM rats did not show a significant variation along the L/D cycle. PINX rats, however, showed a daily profile characterized by a peak at ZT21 (Fig. 4D).

The daily profile of *perk* expression in SHAM and PINX rats showed a significant variation along L/D cycle. The lowest and highest levels of *perk* mRNA expression in SHAM rats were observed at ZT18 and ZT6, respectively ($P < 0.05$). The diurnal profiles were similar in SHAM and PINX rats; the only significant difference was seen at the ZT6 ($P < 0.05$) (Fig. 4E).

There was a significant difference between the 24-h mean of the *xbp-1* mRNA expression in the liver so that PINX values were higher than those of SHAM (Mann-Whitney *U* test; $P < 0.05$). In these two groups, *xbp-1* expression showed a significant variation along the L/D cycle. The highest expression of *xbp-1* mRNA in SHAM rats was observed at ZT24, whereas in PINX rats, it was phase advanced to ZT15. As a consequence, *xbp-1* expression in PINX was reduced at ZT24 (0.60-fold of SHAM values; $P < 0.05$) and increased at ZT12 and ZT15 when compared with SHAM rats (1.50- and 1.80-fold of SHAM values, respectively; $P < 0.05$) (Fig. 4F). Splicing of *xbp-1* mRNA was assessed in key time points. Our data show that in both SHAM and PINX rats, the splicing of *xbp-1* mRNA displayed a biphasic pattern peaking at ZT12 and ZT24. However, it was higher in liver of PINX rats at ZT12 (1.22-fold of SHAM; $P < 0.05$) (Supplemental Fig. 2).

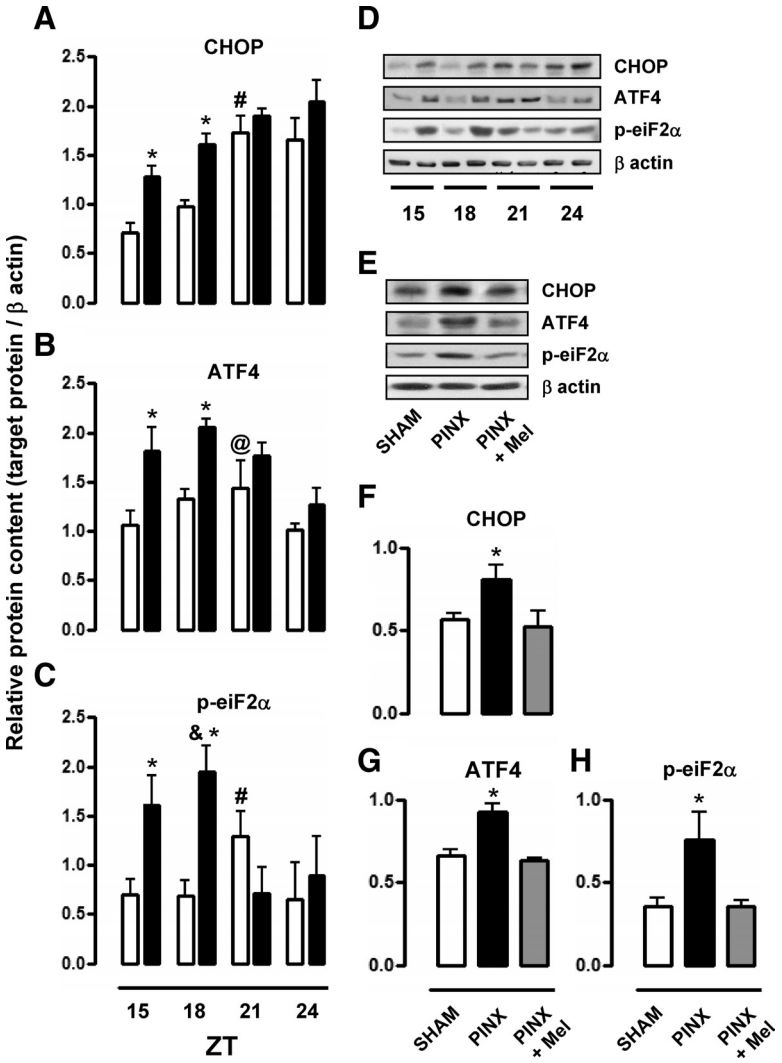

FIG. 5. Nocturnal profile of CHOP and ATF4 content and eiF2α phosphorylation in liver of SHAM and PINX rats. SHAM (*white bars*) and PINX (*black bars*) rats were housed in 12-h light, 12-h dark cycle under *ad libitum* feeding conditions and killed at the indicated ZT times (ZT15, ZT18, ZT21, and ZT24). A fragment of the liver was removed and processed for immunoblotting detection of CHOP, ATF4, phospho (p)-eiF2α, and β-actin (D). Data of CHOP (A), ATF4 (B), and p-eiF2α (C) were normalized by those of β-actin. PINX+Mel rats (*gray bars*) were killed at ZT18, and a fragment of the liver was removed and processed for immunoblotting detection of CHOP, ATF4, p-eiF2α, and β-actin. In this case, SHAM and PINX rats killed at ZT18 were treated with vehicle (E). Data of CHOP (F), ATF4 (G), and p-eiF2α (H) were normalized by those of β-actin. Results are shown as mean ± SE. *, $P < 0.05$ *vs.* SHAM at the same ZT; #, $P < 0.05$ *vs.* SHAM at ZT15; @, $P < 0.05$ *vs.* SHAM at ZT24; &, $P < 0.05$ *vs.* PINX at ZT21 (n = 5).

Absence of Mel increases night-time hepatic CHOP and ATF4 protein content, and eiF2α phosphorylation

CHOP content reached the highest levels at ZT21 in SHAM (2.10-fold of ZT15; $P < 0.05$). However, CHOP content at ZT15 and ZT18 was higher in PINX when compared with SHAM at the same ZT (1.60-fold for both; $P < 0.05$) (Fig. 5A). Administration of Mel to

PINX rats recovered hepatic CHOP content at ZT18 to values similar that found in SHAM rats (Fig. 5F).

ATF4 content progressively increased in SHAM rats from ZT15 up to ZT21, followed by a reduction at ZT24 (at ZT21 was 1.73-fold of SHAM at ZT24, $P < 0.05$). In addition, ATF4 values in PINX rats were higher than in SHAM at ZT15 and ZT18 (1.70- and 1.40-fold, respectively; $P < 0.05$) (Fig. 5B). Mel reduced hepatic ATF4 content at ZT18 so that its levels became similar to that found in SHAM (Fig. 5G).

Phosphorylation of eiF2α peaked at ZT21 in SHAM animals (2.04-fold of ZT15; $P < 0.05$). The highest levels of eiF2α phosphorylation in PINX rats were phase advanced to ZT18 (2.80-fold of ZT21; $P < 0.05$). In addition, eiF2α phosphorylation was higher in PINX than in SHAM at ZT15 and at ZT18 (2.32- and 2.85-fold, respectively; $P < 0.05$) (Fig. 5C). PINX rats treated with Mel showed a reduction of eiF2α phosphorylation at ZT18 so that its levels became similar to that found in SHAM (Fig. 5H).

Absence of Mel changes hepatic TRB3 and RAPTOR expression profiles

Expression of *trb3* and *raptor* was assessed in liver of SHAM and PINX rats during the dark phase of the L/D cycle and at a representative diurnal ZT (ZT6). Maximal values of nocturnal *trb3* mRNA in SHAM rats occurred at ZT12 (3.40-fold of ZT15; $P < 0.05$). On the other hand, in PINX rats, maximal values of *trb3* was phase delayed, occurring at ZT18 (1.79-fold of ZT21, $P < 0.05$). In addition, *trb3* mRNA was reduced in PINX at ZT12 (0.67-fold of SHAM; $P < 0.05$) and increased at ZT18 (1.90-fold of SHAM; $P < 0.05$). At ZT6, *tbr3* expression increased in both SHAM and PINX when compared with their counterparts at ZT24 and was higher in SHAM when comparing with PINX at ZT6 (1.75-fold; $P < 0.05$) (Fig. 6A). TRB3 protein content was also increased in liver of PINX rats at ZT18 when compared with SHAM animals (1.56-fold; $P < 0.05$). Moreover, supplementation with Mel reduced hepatic TRB3 content in PINX rats at ZT18 in such way that it reached values similar to that found in SHAM (Fig. 6D).

Expression of *raptor* mRNA peaked at ZT6 in SHAM rats (5.04-fold of ZT24; $P < 0.05$) and at ZT18 in PINX rats (2.00-fold of ZT24; $P < 0.05$). PINX by itself increased *raptor* mRNA at ZT12, ZT15, ZT18, and ZT24 when compared with their respective SHAM counterparts (1.30-, 1.50-, 1.53-, and 2.25-fold, respectively; $P < 0.05$) but decreased it at ZT6 (0.55-fold of SHAM at ZT6) (Fig. 6B). We have also found that PINX increased hepatic RAPTOR content at ZT18 (1.66-fold the values of SHAM; $P < 0.05$) and Mel reposition reduced it (Fig. 6E).

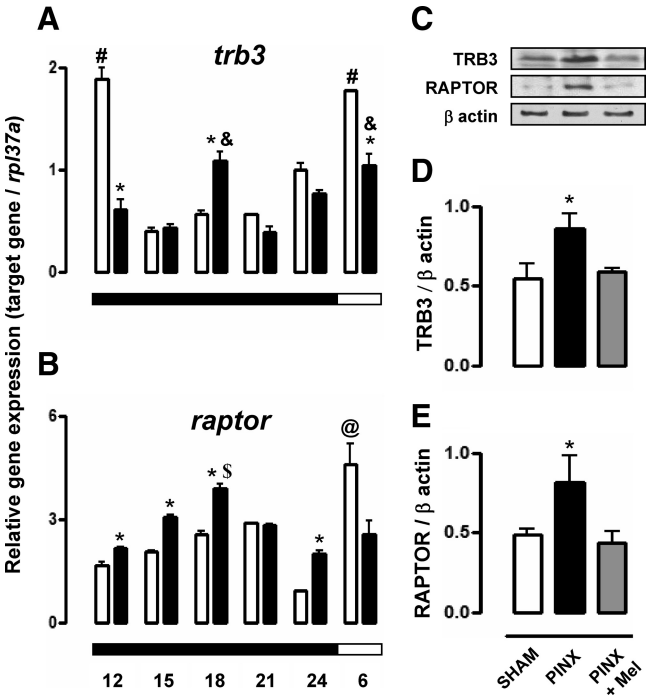

FIG. 6. Nocturnal profile of *trb3* and *raptor* expression in liver of SHAM and PINX rats. SHAM (*white bars*) and PINX (*black bars*) rats were housed in 12-h light, 12-h dark cycle under *ad libitum* feeding conditions and killed at the indicated ZT times (ZT6, ZT12, ZT15, ZT18, ZT21, and ZT24). A fragment of the liver was removed and processed for total RNA extraction and *trb3* (A) and *raptor* (B) mRNAs detection by real-time PCR. SHAM, PINX, and PINX+Mel rats (*gray bars*) were also killed at ZT18, and a fragment of the liver was removed and processed for immunoblotting detection of TRB3, RAPTOR, and β-actin. In this case, SHAM and PINX rats were treated with vehicle (C). Data of TRB3 (D) and RAPTOR (E) were normalized by those of β-actin. Results are shown as mean ± SEM. *, $P < 0.05$ *vs.* SHAM at the same ZT; #, $P < 0.05$ *vs.* SHAM at ZT15; &, $P < 0.05$ *vs.* PINX at ZT21; @, $P < 0.05$ *vs.* SHAM at ZT24; $, $P < 0.05$ *vs.* PINX at ZT24 (n = 4).

PBA treatment improves hepatic insulin action and decreases gluconeogenesis in PINX at ZT24

As shown in Fig. 2A, PINX rats exhibited a higher increase in glucose levels after a pyruvate load when compared with SHAM animals. PINX rats treated with PBA, a chemical chaperone known to inhibit UPR, exhibited values of glycemia after pyruvate injection similar to that found in SHAM (Fig. 7A). The AUC of PINX rats (2.55-fold values of that of SHAM; $P < 0.05$) was completely abrogated by treatment of PINX rats with PBA (Fig. 7B).

No changes in basal AKT phosphorylation were found when comparing SHAM and PINX, but PBA reduced basal AKT phosphorylation of PINX rats (0.30-fold values of basal PINX; $P < 0.05$). In addition, insulin efficiently stimulated AKT phosphorylation in all groups (2.34-fold of respective basal for SHAM, 1.83-fold of respective basal for PINX, and 8.39-fold of respective basal for PINX treated with PBA; $P < 0.05$). Insulin-stimulated AKT phosphorylation in PINX rats was lower than that of SHAM animals (0.66-fold of insulin-stimulated

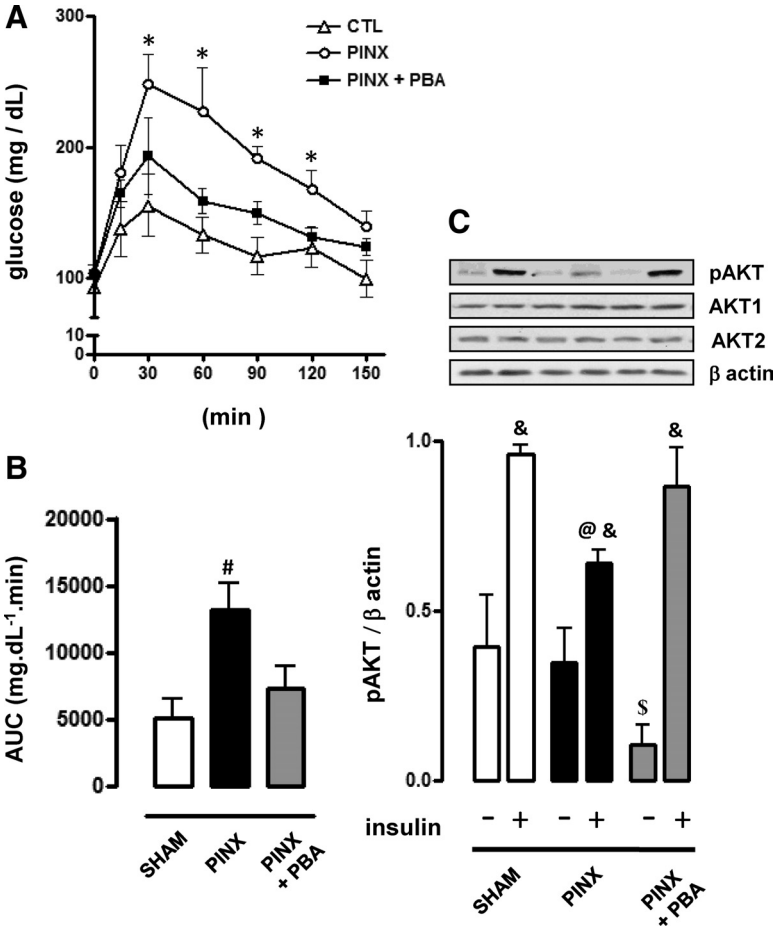

FIG. 7. Gluconeogenesis and insulin-stimulated AKT phosphorylation in liver of SHAM, PINX, and PINX+PBA rats. Intraperitoneal PTT was performed in SHAM, PINX, and PINX+PBA rats at ZT24. Blood was collected from the tail before (0 min) and 15, 30, 60, 90, 120, and 150 min after pyruvate injection (A). The AUC was calculated for each individual animal (B). SHAM, PINX, and PINX+PBA rats were anesthetized, and a fragment of the liver was removed at ZT24. Insulin injection was given in the cava vein, and another liver fragment was removed 30 sec later. Samples were used for immunoblotting detection of pAKT, AKT1, AKT2, and β-actin. Data of pAKT was normalized by those of β-actin (C). Results are shown as mean ± SE. *, $P < 0.05$ *vs.* SHAM at the same time point after pyruvate load; #, $P < 0.05$ *vs.* SHAM; &, $P < 0.05$ *vs.* basal pAKT within the same group; @, $P < 0.05$ *vs.* insulin stimulated pAKT of SHAM; $, $P < 0.05$ *vs.* basal phosphoAKT of PINX (n = 6). CTL, Control.

SHAM; $P < 0.05$). Insulin-stimulated AKT phosphorylation values in PINX rats were recovered to values similar to that found in SHAM animals after treatment with PBA (Fig. 7C).

Discussion

Pineal gland removal is known to result in glucose intolerance by inducing insulin resistance (1). Because a reduced insulin-stimulated glucose uptake by adipocytes of PINX rats occurs independently of the L/D cycle (2), this alteration would not explain the specific increase in night-time circulating glucose values detected after PINX (3).

The daily rhythm of hepatic PEPCK expression and blood glucose levels have been demonstrated to be generated by both nocturnal feeding behavior and oscillations in sympathetic and parasympathetic inputs from the central nervous system to the liver. These conclusions came from studies showing that complete hepatic denervation combined with a noncircadian feeding regimen abolished the night-time reduction in PEPCK expression (6, 7). Our present data add relevant information to the literature in such way that it describes a hormonal signal to the liver that modulates the circadian rhythm of PEPCK. Thus, we do not propose that Mel generates the circadian rhythm of PEPCK but collaborates to keep hepatic PEPCK levels down-regulated until the end of the dark phase.

The most accepted intracellular mechanism that explains how activation of AKT by insulin suppresses PEPCK expression involves FoxO1 phosphorylation (20). FoxO1 is a transcriptional factor that binds to the promoter region of the PEPCK gene and enhances its transcription (21). Once phosphorylated by AKT, FoxO1 translocation to the nucleus is inhibited, resulting in its accumulation in the cytoplasm (21).

We have found increased *foxo1* in SHAM animals at ZT21, which is probably contributing to a posterior increase of *pepck* expression at the diurnal ZT6. In PINX animals, the increase of *foxo1* was phase advanced to ZT18, which is probably contributing to the early increase in *pepck* at ZT24. Reduced basal AKT phosphorylation was also detected in PINX rats at ZT18 and, thus, preceding the increased *pepck*. Considering this, our results suggest that the absence of Mel promotes a phase advance in the night-time increase of *foxo1* with a parallel reduction of AKT phosphorylation (at ZT18). These events possibly favor the increased *pepck* expression in the dark-phase (ZT21 and ZT24). Favoring the hypothesis that Mel might facilitate hepatic night-time insulin action, Mel receptors were shown to be expressed in rat liver (22), and Mel treatment was described to activate AKT *in vivo* (23) and *in vitro* (24). However, because PINX rats have higher corticosterone levels (2), we cannot discard that glucocorticoids may contribute to the hepatic insulin resistance.

To confirm whether these changes would correlate with proper insulin resistance and increased gluconeogenesis in PINX at the end of the night, we next investigated insulin-

stimulated hepatic AKT phosphorylation and whole body gluconeogenesis. Concordantly with increased PEPCK expression at ZT24, liver of PINX rats displayed insulin-resistance as evidenced by reduced insulin-stimulated AKT phosphorylation. The physiological relevance of this alteration was characterized by increased conversion of pyruvate to glucose. In this way, insulin, which is normally high in nocturnal feeding periods, probably does not effectively repress PEPCK and gluconeogenesis in liver of PINX rats. These alterations found in PINX rats are probably due to the absence of Mel, because Mel supplementation reduced PEPCK and gluconeogenesis and increased insulin-stimulated AKT phosphorylation. It is important to note that the night-time hepatic insulin resistance with concomitant increased gluconeogenesis in PINX rats was achieved without changes in body weight and adiposity (Supplemental Table 3).

Attempting to clarify the mechanisms leading to night-time hepatic insulin resistance in liver of PINX rats, we investigated the circadian variation of UPR activation, because this response is being currently considered a crucial event that contributes to insulin resistance throughout the establishment of type 2 diabetes mellitus (11, 25).

Activation of UPR is triggered by the dissociation of the chaperone BiP from the transducer proteins PERK, ATF6 and inositol-requiring protein 1 (IRE1). IRE1 activation targets alternative splicing of *xbp1* mRNA. In mammal cells, processed *xbp1* mRNA originates an active transcription factor that facilitates the expression of several enzymes that promote ER-associated degradation of misfolded proteins (26). ATF6 pathway is somehow redundant to that of IRE1/X-box binding protein 1 but also potentiates IRE1 pathway by increasing the transcription *xbp1* gene (27). PERK activation, in turn, targets eIF2α phosphorylation, which contributes to attenuation of mRNA translation (9).

UPR activation has been described to generate insulin resistance in skeletal muscle and adipose tissue (25, 28). Regarding the liver, long- and short-term activation of the UPR pathways with thapsigargin cause hepatic insulin resistance and stimulate glucose production by gluconeogenesis *in vivo* (13) and correlate with increased PEPCK expression *in vitro* (14). However, the simple affirmation that UPR activation stimulates gluconeogenesis and hepatic insulin resistance is probably not true. Although ATF6 knockout mice develop lower levels of glycemia and reduced PEPCK expression in the liver, these animals are hypersensitive to glucagon-induced gluconeogenesis (29). In this way, the duration of the stress response seems to determine whether UPR will stimulate or inhibit gluconeogenesis by the hepatocyte. Seo *et al.* (14) have demonstrated that acute stimulation with thapsigargin rapidly stimulates ER stress, which favors PEPCK and glucose-6-phosphatase expression. If UPR activation persists, these authors show that the response switches to an inhibition over gluconeogenic enzymes (14). Another independent group has also demonstrated that short-term activation of UPR with chemical agents increases glucose output from hepatic cells (30). Therefore, the current knowledge suggests that a broad and transitory activation of the UPR, rather than chronic activation, favors PEPCK expression and stimulates gluconeogenesis. Importantly, we have found that *atf4, atf6, chop, and bip* expression and eiF2α phosphorylation are up-regulated in liver of PINX rats during intermediary nocturnal time points of the L/D cycle. We have also found increased *xbp-1* splicing in PINX rats at the transition from the light to the dark phase (ZT12) (Supplemental Fig. 2). Thus, it is possible that the oscillatory pattern of UPR activation in liver of PINX rats (what confers a short-term nature) might culminate in increased gluconeogenesis and insulin resistance found at the end of the dark-phase.

To test this hypothesis, we next measured gluconeogenesis and insulin-stimulated AKT phosphorylation in liver of PINX rats treated with PBA, a short chain fatty acid described as a chemical chaperone because of its ability to stabilize protein conformation, to improve ER folding capacity, and to facilitate the trafficking of mutant

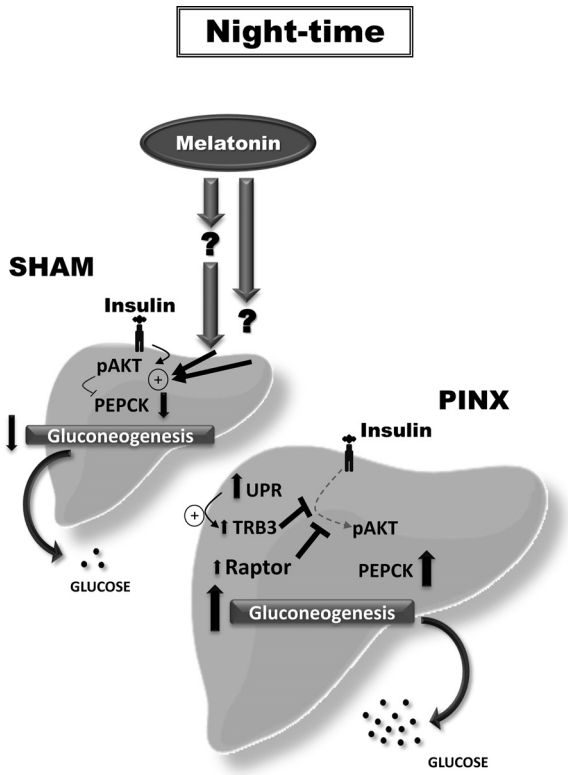

FIG. 8. Diagram representing the proposed model for night-time insulin resistance in liver of PINX rats. AKT, Ras-like protein TC25-α serine/threonine kinase. pAKT, PhosphoAKT.

proteins (31). Importantly, PBA was already demonstrated to inhibit ER stress and improve glucose intolerance by enhancing AKT phosphorylation in liver (32). Favoring the proposition that UPR might cope with insulin resistance and increased gluconeogenesis in liver of PINX rats at the end of the night feeding period, our data show that PBA treatment restores insulin-stimulated AKT phosphorylation in PINX rats and reduces pyruvate conversion to glucose.

TRB3, a pseudo kinase inhibitor of AKT, is a prominent candidate to link UPR to hepatic insulin resistance. Convergent data have shown that increased TRB3 expression in liver of insulin-resistant mice abrogates AKT phosphorylation and stimulates gluconeogenesis (33). In agreement with these findings, we found that *trb3* mRNA expression increases at ZT18 in PINX rats, which correlates with a reduction in AKT phosphorylation. Importantly, Mel supplementation reduced TRB3 protein levels in liver of PINX rats.

UPR stimulation of TRB3 expression was demonstrated to be mediated by a heterodimer formed by ATF4 and CHOP (34). In accordance with this mechanism, we found that the absence o Mel elicits a simultaneous increase of ATF4 and CHOP at ZT15, which precedes the simultaneous raise in TRB3 and the fall in AKT phosphorylation at ZT18. Altogether, our results suggest that the absence of pineal Mel results in an increase of CHOP/ATF4 at ZT15, which, in turn, induces TRB3 expression at ZT18 that will reflect on hepatic insulin resistance fully established at ZT24 (characterized by reduced insulin-stimulated AKT phosphorylation and increased PEPCK and gluconeogenesis).

AKT phosphorylation status is regulated by a myriad of proteins that are beyond the UPR-induced TRB3 expression. For instance, AKT is negatively regulated by RAPTOR, a protein that is able to bind to mTOR forming a complex known as transducer of regulated cAMP response element 1 (35). In liver, forced expression of a nonfunctional RAPTOR was described to increase AKT phosphorylation (36). Our results show a consonant increase of *raptor* mRNA in liver of PINX rats at ZT18. In addition, *raptor* expression is increased in PINX rats at almost all nocturnal ZTs, including ZT24, when insulin resistance was actually detected. Thus, we hypothesize that, together with increased TRB3 expression, an increase in RAPTOR favors the reduction of AKT phosphorylation in liver of PINX rats at the end of the night.

Besides the hepatic night-time insulin resistance induced by PINX, the present data reveal that the absence of Mel causes a putative desynchronization of the gluconeogenic state of the liver from feeding status. As seen in SHAM animals, *pepck* expression increases at the diurnal ZT6 comparing with the last nocturnal time point and reaches a maximum at ZT12 just prior lights off. This increase in *pepck* parallels the minimal diurnal food intake of SHAM animals, being almost all food intake occurring during the night (when *pepck* expression is progressively repressed). Exactly as for SHAM, PINX maintained this preferential nocturnal food behavior (Supplemental Fig. 1), but in these animals, hepatic *pepck* tends to diminish as they went from ZT24 to ZT6. Our interpretation is that the absence of Mel might impair glucose metabolism not only by causing insulin resistance but also by disrupting the entrainment of food intake and hepatic glucose production. Favoring this hypothesis, PINX rats show reduced hepatic *trb3, foxo1,* and raptor expression at ZT6. We would like to stress, however, that this desynchronization remains to be consistently demonstrated.

In summary, this work shows that the absence of Mel prompts hepatic insulin resistance at the end of the night feeding period, highlighted by reduced insulin-stimulated AKT phosphorylation and increased gluconeogenesis and PEPCK expression. This phenomenon is probably a result of UPR activation and stimulation of *trb3* expression during intermediary hours of the dark phase of L/D cycle (ranging from ZT15 to ZT21). Moreover, increased expression of RAPTOR is also likely to contribute to insulin resistance. A summary diagram of our data is shown in Fig. 8. To our knowledge, this study is the first to report circadian alterations in hepatic UPR activation and to relate these changes with Mel absence and night-time insulin resistance.

Acknowledgments

We thank technical assistance of Mr. José Luiz dos Santos and Mrs. Julieta Scialfa Falcão. We also thank Dr. Licio A. Velloso for providing part of antibodies used in the study.

Address all correspondence and requests for reprints to: Dr. Gabriel Forato Anhê, Department of Pharmacology, Faculty of Medical Sciences, State University of Campinas, Alexander Fleming Street 101, Campinas 13084-971, Brazil. E-mail: anhegf@fcm.unicamp.br.

This work was supported by Brazilian foundations Fundação de Amparo a Pesquisa do Estado de São Paulo, Conselho Nacional de Pesquisa, and Coordenação de Aperfeiçoamento de Pessoal de Nível Superior.

Disclosure Summary: The authors have nothing to disclose.

References

1. **Lima FB, Machado UF, Bartol I, Seraphim PM, Sumida DH, Moraes SM, Hell NS, Okamoto MM, Saad MJ, Carvalho CR, Cipolla-Neto**

J 1998 Pinealectomy causes glucose intolerance and decreases adipose cell responsiveness to insulin in rats. Am J Physiol 275:E934–E941

2. **Alonso-Vale MI, Borges-Silva CN, Anhê GF, Andreotti S, Machado MA, Cipolla-Neto J, Lima FB** 2004 Light/dark cycle-dependent metabolic changes in adipose tissue of pinealectomized rats. Horm Metab Res 36:474–479
3. **la Fleur SE, Kalsbeek A, Wortel J, van der Vliet J, Buijs RM** 2001 Role for the pineal and melatonin in glucose homeostasis: pinealectomy increases night-time glucose concentrations. J Neuroendocrinol 13:1025–1032
4. **Picinato MC, Haber EP, Carpinelli AR, Cipolla-Neto J** 2002 Daily rhythm of glucose-induced insulin secretion by isolated islets from intact and pinealectomized rat. J Pineal Res 33:172–177
5. **Granner D, Andreone T, Sasaki K, Beale E** 1983 Inhibition of transcription of the phosphoenolpyruvate carboxykinase gene by insulin. Nature 305:549–551
6. **Cailotto C, La Fleur SE, Van Heijningen C, Wortel J, Kalsbeek A, Feenstra M, Pévet P, Buijs RM** 2005 The suprachiasmatic nucleus controls the daily variation of plasma glucose via the autonomic output to the liver: are the clock genes involved? Eur J Neurosci 22:2531–2540
7. **Cailotto C, van Heijningen C, van der Vliet J, van der Plasse G, Habold C, Kalsbeek A, Pévet P, Buijs RM** 2008 Daily rhythms in metabolic liver enzymes and plasma glucose require a balance in the autonomic output to the liver. Endocrinology 149:1914–1925
8. **Radziuk J, Pye S** 2006 Diurnal rhythm in endogenous glucose production is a major contributor to fasting hyperglycaemia in type 2 diabetes. Suprachiasmatic deficit or limit cycle behaviour? Diabetologia 49:1619–1628
9. **Ron D, Walter P** 2007 Signal integration in the endoplasmic reticulum unfolded protein response. Nat Rev Mol Cell Biol 8:519–529
10. **Hotamisligil GS** 2008 Inflammation and endoplasmic reticulum stress in obesity and diabetes. Int J Obes 32(Suppl 7):S52–S54
11. **Eizirik DL, Cardozo AK, Cnop M** 2008 The role for endoplasmic reticulum stress in diabetes mellitus. Endocr Rev 29:42–61
12. **Nakatani Y, Kaneto H, Kawamori D, Yoshiuchi K, Hatazaki M, Matsuoka TA, Ozawa K, Ogawa S, Hori M, Yamasaki Y, Matsuhisa M** 2005 Involvement of endoplasmic reticulum stress in insulin resistance and diabetes. J Biol Chem 280:847–851
13. **Gonzales JC, Gentile CL, Pfaffenbach KT, Wei Y, Wang D, Pagliassotti MJ** 2008 Chemical induction of the unfolded protein response in the liver increases glucose production and is activated during insulin-induced hypoglycaemia in rats. Diabetologia 51:1920–1929
14. **Seo HY, Kim MK, Min AK, Kim HS, Ryu SY, Kim NK, Lee KM, Kim HJ, Choi HS, Lee KU, Park KG, Lee IK** 2010 Endoplasmic reticulum stress-induced activation of activating transcription factor 6 decreases cAMP-stimulated hepatic gluconeogenesis via inhibition of CREB. Endocrinology 151:561–568
15. **Martins Jr E, Ligeiro de Oliveira AP, Fialho de Araujo AM, Tavares de Lima W, Cipolla-Neto J, Costa Rosa LF** 2001 Melatonin modulates allergic lung inflammation. J Pineal Res 31:363–369
16. **Mauriz JL, Molpeceres V, García-Mediavilla MV, González P, Barrio JP, González-Gallego J** 2007 Melatonin prevents oxidative stress and changes in antioxidant enzyme expression and activity in the liver of aging rats. J Pineal Res 42:222–230
17. **Caperuto LC, Anhê GF, Cambiaghi TD, Akamine EH, do Carmo Buonfiglio D, Cipolla-Neto J, Curi R, Bordin S** 2008 Modulation of bone morphogenetic protein-9 expression and processing by insulin, glucose, and glucocorticoids: possible candidate for hepatic insulin-sensitizing substance. Endocrinology 149:6326–6335
18. **Ramakers C, Ruijter JM, Deprez RH, Moorman AF** 2003 Assumption-free analysis of quantitative real-time polymerase chain reaction (PCR) data. Neurosci Lett 339:62–66
19. **Liu W, Saint DA** 2002 A new quantitative method of real time reverse transcription polymerase chain reaction assay based on simulation of polymerase chain reaction kinetics. Anal Biochem 302:52–59
20. **Yeagley D, Guo S, Unterman T, Quinn PG** 2001 Gene- and activation-specific mechanisms for insulin inhibition of basal and glucocorticoid-induced insulin-like growth factor binding protein-1 and phosphoenolpyruvate carboxykinase transcription. Roles of forkhead and insulin response sequences. J Biol Chem 276:33705–33710
21. **Taniguchi CM, Emanuelli B, Kahn CR** 2006 Critical nodes in signalling pathways: insights into insulin action. Nat Rev Mol Cell Biol 7:85–96
22. **Sallinen P, Saarela S, Ilves M, Vakkuri O, Leppäluoto J** 2005 The expression of MT1 and MT2 melatonin receptor mRNA in several rat tissues. Life Sci 76:1123–1134
23. **Anhê GF, Caperuto LC, Pereira-Da-Silva M, Souza LC, Hirata AE, Velloso LA, Cipolla-Neto J, Carvalho CR** 2004 In vivo activation of insulin receptor tyrosine kinase by melatonin in the rat hypothalamus. J Neurochem 90:559–566
24. **Alonso-Vale MI, Andreotti S, Peres SB, Anhê GF, das Neves Borges-Silva C, Neto JC, Lima FB** 2005 Melatonin enhances leptin expression by rat adipocytes in the presence of insulin. Am J Physiol Endocrinol Metab 288:E805–E812
25. **Boden G, Duan X, Homko C, Molina EJ, Song W, Perez O, Cheung P, Merali S** 2008 Increase in endoplasmic reticulum stress-related proteins and genes in adipose tissue of obese, insulin-resistant individuals. Diabetes 57:2438–2444
26. **Yoshida H, Matsui T, Hosokawa N, Kaufman RJ, Nagata K, Mori K** 2003 A time-dependent phase shift in the mammalian unfolded protein response. Dev Cell 4:265–271
27. **Yoshida H, Matsui T, Yamamoto A, Okada T, Mori K** 2001 XBP1 mRNA is induced by ATF6 and spliced by IRE1 in response to ER stress to produce a highly active transcription factor. Cell 107:881–891
28. **Srinivasan V, Tatu U, Mohan V, Balasubramanyam M** 2009 Molecular convergence of hexosamine biosynthetic pathway and ER stress leading to insulin resistance in L6 skeletal muscle cells. Mol Cell Biochem 328:217–224
29. **Wang Y, Vera L, Fischer WH, Montminy M** 2009 The CREB coactivator CRTC2 links hepatic ER stress and fasting gluconeogenesis. Nature 460:534–537
30. **Wang D, Wei Y, Schmoll D, Maclean KN, Pagliassotti MJ** 2006 Endoplasmic reticulum stress increases glucose-6-phosphatase and glucose cycling in liver cells. Endocrinology 147:350–358
31. **Welch WJ, Brown CR** 1996 Influence of molecular and chemical chaperones on protein folding. Cell Stress Chaperon 1:109–115
32. **Ozcan U, Yilmaz E, Ozcan L, Furuhashi M, Vaillancourt E, Smith RO, Görgün CZ, Hotamisligil GS** 2006 Chemical chaperones reduce ER stress and restore glucose homeostasis in a mouse model of type 2 diabetes. Science 313:1137–1140
33. **Du K, Herzig S, Kulkarni RN, Montminy M** 2003 TRB3: a tribbles homolog that inhibits Akt/PKB activation by insulin in liver. Science 300:1574–1577
34. **Ohoka N, Yoshii S, Hattori T, Onozaki K, Hayashi H** 2005 TRB3, a novel ER stress-inducible gene, is induced via ATF4-CHOP pathway and is involved in cell death. EMBO J 24:1243–1255
35. **Sarbassov DD, Guertin DA, Ali SM, Sabatini DM** 2005 Phosphorylation and regulation of Akt/PKB by the rictor-mTOR complex. Science 307:1098–1101
36. **Koketsu Y, Sakoda H, Fujishiro M, Kushiyama A, Fukushima Y, Ono H, Anai M, Kikuchi T, Fukuda T, Kamata H, Horike N, Uchijima Y, Kurihara H, Asano T** 2008 Hepatic overexpression of a dominant negative form of raptor enhances Akt phosphorylation and restores insulin sensitivity in K/KAy mice. Am J Physiol Endocrinol Metab 294:E719–E725